

RSC Advances



This is an *Accepted Manuscript*, which has been through the Royal Society of Chemistry peer review process and has been accepted for publication.

Accepted Manuscripts are published online shortly after acceptance, before technical editing, formatting and proof reading. Using this free service, authors can make their results available to the community, in citable form, before we publish the edited article. This *Accepted Manuscript* will be replaced by the edited, formatted and paginated article as soon as this is available.

You can find more information about *Accepted Manuscripts* in the [Information for Authors](#).

Please note that technical editing may introduce minor changes to the text and/or graphics, which may alter content. The journal's standard [Terms & Conditions](#) and the [Ethical guidelines](#) still apply. In no event shall the Royal Society of Chemistry be held responsible for any errors or omissions in this *Accepted Manuscript* or any consequences arising from the use of any information it contains.

Novel nanocomposite membranes based on blended sulfonated poly(ether ether ketone)/poly(vinyl alcohol) containing sulfonated graphene oxide/Fe₃O₄ nanosheets for DMFC applications

Hossein Beydaghi,^{a,b} Mehran Javanbakht,^{*a,b} Ahmad Bagheri,^{a,b} Parisa Salarizadeh,^{a,b} Hossein Ghafarian- Zahmatkesh,^{a,b} Sepideh Kashefi^c and Elaheh Kowsari^a

^a Department of Chemistry, Amirkabir University of Technology, Tehran, 1599637111, Iran

^b Fuel Cell and Solar Cell Laboratory, Renewable Energy Research Center, Amirkabir University of Technology, Tehran, 1599637111, Iran

^c Department of Chemical Engineering, Semnan University, Semnan, 35195363, Iran

Abstract

In this study, the Sulfonated graphene oxide (SGO)/Fe₃O₄ nanosheets were synthesized by hydrothermal method and incorporated into blend sulfonated poly(ether ether ketone) (SPEEK)/poly(vinyl alcohol) (PVA) matrix with different weight percent of (SGO)/Fe₃O₄ nanosheets. The performances of prepared membranes were investigated by water uptake, membrane swelling, mechanical and thermal stability, proton conductivity, methanol permeability and DMFC test. It was found that the water uptake and tensile strength of SPEEK membrane increased and proton conductivity and power density decreased by

* Corresponding author at: Department of Chemistry, Amirkabir University of Technology, Tehran, Iran. Tel.: +98 21 64542764; fax: +98 21 64542762. *E-mail address*: mehranjavanbakht@gmail.com (M. Javanbakht).

blending with PVA. Incorporation of SGO/Fe₃O₄ nanosheets into SPEEK/PVA matrix enhanced mechanical stability, proton conductivity and methanol barrier properties of membrane. The SPEEK/PVA/SGO/Fe₃O₄ nanocomposite membrane with optimal nanosheets content (5 wt%) exhibits low methanol permeability ($8.83 \times 10^{-7} \text{ cm}^2 \text{ s}^{-1}$), high tensile strength (51.2 MPa), high proton conductivity (0.084 S cm^{-1} at 25°C) and high power density (122.7 mW cm^{-2} at 80°C) and suggests its potential application in DMFCs.

Introduction

Direct methanol fuel cells (DMFC) are one type of fuel cells that attracted huge attention for portable uses in recent years. Some of DMFCs advantages are high energy density, liquid state of methanol, needless to any reformer, low pollution, safe storage instead of hydrogen, and near-room operating temperature.¹⁻³ Although DMFCs have lots of advantages but their usage faces with some challenges such as methanol crossover from membrane. It must be mentioned that, proton exchange membrane (PEM) plays an important role as essential component of DMFCs.^{4,5} In recent years researchers have focused on preparing membranes with high performance. The important points for improving the DMFCs performances are high proton conductivity and low methanol permeability. Methanol crossover from the anode to the cathode through the PEM and cause poisoning in the cathode and hence reduce current density and fuel cell performance.^{6,7} In most application of DMFCs, it's common to use perfluorinated membranes such as Nafion. The high proton conductivity, flexibility, and good chemical stability are some advantages that considered for this type of membranes.^{8,9} Besides this advantages, the Nafion membranes have some disadvantage that are important for DMFCs application, such as high methanol crossover, low proton conductivity at temperature above 80°C, and high cost that caused researchers to focus on preparation of alternative

membranes.^{10,11} In recent years many researches have been occurred on preparation of blend and composite membrane by usage of inorganic material such as $\text{La}_2\text{Ce}_2\text{O}_7$,¹² Fe_2TiO_5 ,¹³ montmorillonite,¹⁴ silica immobilized phosphotungstic acid (Si-PWA)¹⁵ and alternative organic polymer such as sulfonated polyphthalazinone (SPP),^{16,17} polybenzimidazole (PBI),^{18–}²⁰ sulfonated poly(ether sulfone) (SPES),^{21,22} poly(vinyl alchole) (PVA),^{23,24} sulfonated poly(ether ether ketone) (SPEEK).²⁵ The hydrophilic nature of mentioned inorganic additives helps water uptake and hence proton conductivity increase.

Among these polymers, SPEEK, which is obtained by the electrophilic substitution of sulfonic acid groups in the polymer backbone, is a promising candidate to be used as PEMs in DMFC due to its excellent methanol barrier, good proton conductivity, stability and also low cost compared to Nafion.²⁶ The use of this polymer in last decades represents the importance and advantageous of SPEEK for apply in DMFCs. The properties of SPEEK membrane are depending on degree of sulfonation (DS). Sulfonation of PEEK can be controlled by temperature, acid concentration, and sulfonation time. With increase in DS of SPEEK membranes, proton conductivity improves and mechanical stability and methanol permeability deteriorate.²⁷ In DS of below 60% the proton conductivity of SPEEK membrane is not good for PEMs using in DMFCs. Also, in SPEEK membranes with high DS, the proton conductivity is comparable to that of Nafion membrane, but the mechanical properties deteriorate due to the plasticizing nature of sulfonic acid groups and are thus unsuitable for practical DMFC application. To overcome this drawback, cross-linking is a good idea.²⁶ Cross-linking is an efficient method to limit membrane swelling and methanol permeability and enhances the stability and mechanical properties of membranes. For practical use, these membranes should be modified to improve their stability, which might be realized through blending them with organic and inorganic fillers. Recently, several researchers have

synthesized SPEEK membrane blended with other membranes such as Nafion,²⁸ polystyrene sulfonic acid (PSSA),²⁹ PVA and polyvinyl butyral (PVB).³⁰

One of the best organic polymers for blending with SPEEK is PVA. This polymer has high hydrophilic property, excellent mechanical strength, thermal stability, chemical cross-linking ability, low cost, good water uptake and flexibility.³¹ The large amount of hydroxyl groups in PVA structure improve performing chemical cross-linking with sulfonic acid groups of SPEEK. The good mechanical and thermal properties of PVA polymer and chemical cross-linking reaction between PVA and SPEEK polymers improve mechanical and thermal stability of blend membrane. Also, the hydrophilic nature of PVA, increases water uptake of blend membranes and prevents from intensely decrease of proton conductivity in high temperature.

With blending of SPEEK and PVA water uptake, mechanical and thermal properties improve and proton conductivity decreases. Also, higher water uptake in membrane allows more methanol to pass through along with water in this membrane. For realization of all ideal properties, addition of inorganic fillers to blend membrane is one of the best ideas. Sulfonated graphene oxide (SGO) is one of the most popular nanomaterials that used by researchers in PEMs in recent years.^{27,32} The fuel barrier properties of graphene oxide based nanosheets help to decrease methanol permeability of PEMs used in DMFCs.³² SGO can reinforce mechanical properties and also increase proton conductivity in PEMs by hydrogen bonding between $-OH$, $-SO_3H$ and $-COOH$ groups of available in their structure and $-OH$ and $-SO_3H$ groups of blend membranes.³¹ For improve in performance of blend membrane, the SGO nanosheets decorated with Fe_3O_4 nanoparticles by solvothermal method. The hydrogen bonding between surfaces hydroxyl groups of Fe_3O_4 nanoparticles and free water existing in membrane, help to proton transferring through membrane with Vehicle mechanism and

increased membrane performance. Also, the mechanical stability of blend membranes improved with hydrogen bonding between –OH groups of Fe₃O₄ nanoparticles and –OH and –SO₃H groups of blend membranes. Recently, the orientation of SGO/Fe₃O₄ nanosheets in matrix of PVA membrane by casting in magnetic field for improvement of water uptake, proton conductivity and performance of the nanocomposite membranes was investigated.³³

In this work, for the first time, addition of composite filler (SGO/Fe₃O₄ nanosheets) to cross-linked SPEEK/PVA blend membranes was investigated. The morphology, water uptake, mechanical properties, thermal stability, methanol permeability, proton conductivity, and performance of new nanocomposite blend membranes were investigated and compared with pristine SPEEK membrane. Investigation results demonstrate that the nanocomposite blend membranes possess superior mechanical properties, good dimensional and thermal stability, and improve proton conductivity as well as performance.

Experimental

Materials

Poly(ether ether ketone), PEEK, (M_w=28800 g mol⁻¹, M_n=10300) and Poly(vinyl alcohol), PVA, (degree of hydrolysis, min. 99% and M_w=130000 g mol⁻¹) were purchased from sigma–Aldrich. All other materials and solvents procured from Merck. All chemical materials were used as received without further purification.

Syntheses of sulfonated graphene oxide/Fe₃O₄ nanosheets

Natural graphite was applied to syntheses graphene oxide (GO) via the modified Hummers method.³⁴ The SGO nanosheets were obtained from GO by method mentioned in reference.³¹ To synthesize the Fe₃O₄ nanoparticles, at first, 0.8 g FeCl₃.6H₂O and 0.3 g FeCl₂.4H₂O were

dissolved in deionized water and stirred vigorously. Subsequently, 15 mL NaOH solution was added quickly into the mixture followed by stirring for 2 h at room temperature. Finally, the black colored precipitate was collected on a magnet and washed with deionized water for several times, and then dried in an oven at 60°C.

For preparation of SGO/Fe₃O₄ nanosheets, 80 mg of SGO nanosheets was added into appropriate amount of deionized water followed by sonication for 15 min. Separately, appropriate weight of Fe₃O₄ nanoparticles was dispersed in 120 mL deionized water and sonicated for 15 min. Then, to achieve a homogenous mixture, SGO suspension was added into Fe₃O₄ solution and sonicated for 30 min. After that, for hydrothermal reaction, resulted solution was loaded into Teflon lined stainless steel autoclave at 180°C and stirred for 24 h. At the end of this process, resultant product was washed with deionized water and dried in vacuum oven at 60°C for 24 h.

Sulfonation of PEEK

SPEEK was obtained via direct sulfonation of PEEK. Firstly, PEEK was dried for 24 h in vacuum oven at 60°C before sulfonation. The dried PEEK (1 g) was slowly added into 10 mL concentrated sulfuric acid under vigorous stirring for 1 h at room temperature. After complete dissolution of PEEK, the temperature of solution was raised to 60°C with vigorous stirring for 4 h and then cooled to room temperature. After that, the cooled solution was slowly added to large excess of iced cold water under stirring. The precipitate was then washed with deionized water until neutral pH and then dried at 70°C in a vacuum oven.

The degree of sulfonation (DS) of the SPEEK was determined by ¹H NMR and titration methods. The DS was determined 70% by titration with sodium hydroxide solution. 0.2 g polymer was dissolved in DMF and titrated with a 0.02 M NaOH solution, using phenolphthalein as an indicator. The DS was calculated as follow:

$$DS = \frac{10^{-3} \times 288.31 \times C_{\text{NaOH}} V_{\text{NaOH}}}{W - 0.081 C_{\text{NaOH}} V_{\text{NaOH}}} \times 100$$

where, C_{NaOH} is the molarity of the NaOH solution, V_{NaOH} is the amount of NaOH solution consumed and W is the weight of the sample.

In ^1H NMR method the intensity of the H_E signal was used to determine the SO_3H group content that is equivalent to the DS of SPEEK per repeat unit.³⁵ Hence DS can be calculated by taking the ratios between the peak area of H_E (A_{H_E}) to the peak areas of all the other aromatic hydrogens ($A_{H_{A,A',B,B',C,D}}$). Fig. 1 shows various aromatic protons and ^1H NMR spectrum of SPEEK. DS was calculated using the following formula:³⁵

$$\frac{n}{12 - 2n} = \frac{A_{H_E}}{\sum A_{H_{A,A',B,B',C,D}}}$$

$$DS(\%) = n \times 100$$

where, n is the number of H_E per repeat unit. The DS of the SPEEK was determined 69% that indicates both techniques gave identical results.

Preparation of nanocomposite membranes

Three type of membranes (SPEEK, SPEEK/PVA and SPEEK/PVA/SGO/ Fe_3O_4) were prepared and named M_S , M_{SP} , and M_{SPSFx} respectively, where x present the weight percent of SGO/ Fe_3O_4 nanosheets (3, 5 and 7) in the SPEEK/PVA blend membranes. The membranes with 10 wt% concentration of polymer blend (SPEEK:PVA weight ratio: 60:40) in solution were prepared via solution casting method. Other authors have reported the syntheses of SPEEK/PVA blend membranes and weight ratio of between 35–45 wt% PVA exhibited the best properties in terms of mechanical stability, proton conductivity and methanol permeability.³⁰ For syntheses of M_{SPSFx} membrane, LiCl with a 0.4 wt% concentration was

dissolved in DMAc at room temperature. Incorporation of lithium chloride (LiCl) caused more solubility of PVA in DMAc.³⁶ When LiCl dissolved completely; required amount of PVA was slowly added into solution and stirred for 1 h at 140°C. Separately, appropriate amount of SPEEK was dissolved in DMAc under stirring at room temperature. Before mixing SPEEK and PVA solution and in order to avoid the creation of stress, SPEEK solution was heated to 120°C and stirred for 1 h. Then SPEEK solution was added to PVA solution and stirred at 140°C for 1 h. Finally, appropriate amount of SGO/Fe₃O₄ nanosheets were added to resulting solution and sonicated for 1 h. The resulting solution was cast onto the clean glass plate, successively dried at room temperature for 12 h and 70°C for 12 h, and then 180°C for 3 h to completion of cross-linking process. The other membranes were prepared with same method without presence of other materials. The thickness of the dry membranes is between 100–150 µm. Fig. 2 shows the schematic structure of synthesized nanocomposite membranes. Also, the cross-linking reaction between SPEEK and PVA and interaction between polymer chains and SGO/Fe₃O₄ nanosheets are shown in Fig. 2.

Apparatus

The IR spectra (resolution 4 cm⁻¹) of samples were recorded on a Bruker Equinox 55 with ultra-dry compressed air in the range of 4000–400 cm⁻¹. The ¹H NMR spectra was used to determine the DS of SPEEK using ¹H NMR spectrometer (Bruker 500 MHz). The sample was prepared by dissolving of SPEEK polymer in a dimethylacetamide (DMAc). The crystal structure of nanoparticles and nanosheets was confirmed by X-ray diffraction patterns using X pert pro Philips Diffractometer with Cu K α radiation. The morphology of all samples was examined by AIS2100 Seron Technology scanning electron microscopy (SEM) system and Zeiss EM900 transmission electron microscopy (TEM). The cross sections of prepared membranes were acquired by using the method of liquid nitrogen brittle fracture. The

differential scanning calorimetric (DSC) measurements were performed on the dried samples using a Mettler DSC 823. The scanning rate was $10^{\circ}\text{C min}^{-1}$ in nitrogen flow. The mechanical properties of the membranes were assessed on a SANTAM DBBP-100 testing machine with an operating rate of 1 mm min^{-1} at room temperature. The proton conductivity of all nanocomposite membranes was measured by AC impedance spectroscopy with an Autolab potentiostat/galvanostat with a frequency range of 0.1 Hz–100 kHz and voltage amplitude of 50 mV.

Characterization of membranes

The ion exchange capacity (IEC) of nanocomposite membranes was determined by back-titration method. Firstly, square pieces of each membrane were immersed in 50 mL of 1 M NaCl solution at room temperature for 24 h to exchange the H^+ ions with the Na^+ ions in the solution. After that, solution was titrated with a 0.01 M NaOH solution by using phenolphthalein as an indicator. The value of IEC was determined from following equation:

$$\text{IEC} = \frac{V_{\text{NaOH}} \times C_{\text{NaOH}}}{W_{\text{dry}}} \times 100\%$$

where, V_{NaOH} is consumed volume of NaOH (mL), C_{NaOH} is the concentration of NaOH (mol L^{-1}) and W_{dry} is the weight of the dry membrane (g).

To determine the water uptake (WU) and membrane swelling (SW), the membranes were dried at 100°C for 12 h and then their weights (m_{dry}) and the thickness (L_{dry}) were measured. After that, they were soaked in deionized water for 24 h at room temperature. Finally, the surface water of membranes was blotted with a clean paper and immediately weights (m_{wet}) and thickness (L_{wet}) of membranes were measured. The water uptake and membrane swelling were calculated from following equations:

$$WU (\%) = \frac{m_{wet} - m_{dry}}{m_{dry}} \times 100$$

$$SW (\%) = \frac{L_{wet} - L_{dry}}{L_{dry}} \times 100$$

The proton conductivity of the prepared membranes was tested using an AC impedance spectroscopy. Before test, the membranes were hydrated in deionized water for 24 h until got sufficiently wet and saturated. Hydrated membranes were placed between the two platinum electrodes and membrane resistance was investigated. The proton conductivity was determined from following equation:

$$\sigma = \frac{L}{RA}$$

where, σ is the proton conductivity of the membrane ($S\ cm^{-1}$), L is the thickness of the membrane (cm), R is the resistance of the membrane (Ω), and A is the surface area of the two electrodes (cm^2).

Methanol permeability (P) was evaluated using a glass diffusion cell separated into two compartments. One compartment was filled up with 5 M methanol solution and the other compartment was filled up with deionized water. The nanocomposite membranes were fabricated through two compartments of this apparatus. Before test, the membranes were hydrated for 12 h. Both compartments were under continuous stirring condition during the experiment. Methanol concentration in the water compartment was examined with time using a density meter. The methanol permeability (P) was calculated from following equation:

$$C_B(t) = \frac{A P}{L V_B} C_A (t - t_0)$$

where, C_A and C_B are the concentration of methanol in methanol and water compartment (mol L^{-1}) respectively; L is the thickness of the membranes (cm), A is the diffusion area (cm^2) and V_B is the volume of deionized water in water compartment (mL).

The selectivity factor (S) is an important parameter in direct methanol fuel cell. The selectivity of membranes defined as following equation:

$$S = \frac{\sigma}{P}$$

where, S is the membrane selectivity (S s cm^{-3}), σ is the proton conductivity (S cm^{-1}) and P is the methanol permeability ($\text{cm}^2 \text{s}^{-1}$).

Membrane-electrode assembly (MEA) was prepared via painting method. The catalyst ink was prepared by mixing suitable amount of Pt/Ru/C catalyst with Nafion binder solution, isopropyl alcohol (IPA) and deionized water for the anode ink. The catalyst ink was painted onto carbon cloth (E-tek, HT 2500-W) to give a Pt/Ru loading 2 mg cm^{-2} . The catalyst for the cathode was Pt/C on carbon cloth with a Pt loading of 1 mg cm^{-2} . The MEA fabricated by hot-pressing of prepared membranes with electrodes at 80°C and pressure of 50 kg cm^{-2} for 3 min. The DMFC cell was operated at room temperature. A 1 M methanol was pumped into the anode at a flow rate of 3 mL min^{-1} and pure oxygen gas was supplied to enter the cathode at a flow rate of 300 mL min^{-1} under ambient pressure.

Results and discussion

Structural characterization

XRD analysis was carried out for nanoparticle and nanosheets to confirm the surface modification of SGO nanosheets by Fe_3O_4 nanoparticles. The XRD patterns of prepared samples are presented in Fig. 3. From the XRD profile, it can be seen that there is a sharp

peak overlays on the 2θ of 11.9° and wide peak at 26.3° for GO and SGO nanosheets respectively, which indicates increasing the attractive interaction between the GO layers with sulfonation of GO nanosheets. Addition of SO_3H groups to structure of GO nanosheets decreased crystallinity of GO nanosheets and decreased intensity of 2θ peak in the SGO nanosheets. The increase of 2θ with sulfonation of GO nanosheets decreases interlayer spacing of nanosheets.³⁷ The interlayer spacing in GO nanosheets (0.75 nm) is higher than SGO nanosheets (0.41 nm), calculated using Bragg's law ($\lambda = 2d \sin \theta$). In Fe_3O_4 nanoparticles, the peaks with 2θ values of 30.0° , 35.2° , 43.1° , 53.1° , 56.9° , and 62.3° correspond to the (220), (311), (400), (422), (511), and (440) facets of the crystal planes of Fe_3O_4 nanoparticles.³⁸ For the SGO/ Fe_3O_4 pattern, the relatively low peak shown at 25° confirms the existence of SGO in the structure of SGO/ Fe_3O_4 nanosheets. The little decrease in 2θ , followed by an increase in interlayer spacing of SGO nanosheets with incorporation with Fe_3O_4 is due to entering of Fe_3O_4 nanoparticles between the SGO nanosheets.

Fig. 4 shows the FTIR spectra of SGO/ Fe_3O_4 nanosheets and prepared membranes. In SGO/ Fe_3O_4 spectra, the peaks at 830, 1030, 1114, and 1165 cm^{-1} confirmed existence of phenyl sulfonated groups on the structure of nanosheets.³¹ The peak at 3421 cm^{-1} was assigned to O–H stretching vibration band, and confirmed the presence of hydroxyl groups in nanosheets. The peak at 1631 cm^{-1} was assigned to the C=C skeletal vibration in the unoxidized graphitic domain.³¹ The peak at 587 cm^{-1} ascribed to the stretching vibration of Fe–O groups in Fe_3O_4 nanoparticles.³⁹ In M_S spectra, the peaks which are observed at around 1217 and 1490 cm^{-1} is due to C–O–C and C–C aromatic ring in the SPEEK.⁴⁰ The absorption peaks at 1023, 1074 and 1247 cm^{-1} were assigned to the asymmetric and symmetric stretching vibration of O=S=O and stretching vibration of S=O on sulfonic acid groups in SPEEK.⁴¹ The absorption peak at 1644 cm^{-1} corresponds to the carbonyl groups of SPEEK.⁴¹ The M_{SP} and M_{SPSF5} membranes show an absorption peak around 2920 cm^{-1} assigned to the

symmetric $-\text{CH}_2-$ groups of PVA and a broad peak between $3000\text{--}3500\text{ cm}^{-1}$ due to overlapping of hydroxyl groups from PVA and hydroxyl groups from sulfonic acid groups of SPEEK. The low intensity of this peak is due to direct condensation reaction between sulfonic acid groups of SPEEK and hydroxyl groups of PVA thus establishing cross-linking bonds.³⁰

Fig. 5 shows the SEM and TEM images of SGO (a, b) and SGO/ Fe_3O_4 (c, d) nanosheets. From Fig. 5a and b, sheet-like morphology of SGO nanosheets consisting of wrinkled structures was observed. In Fig. 5c and d, it is interesting to find that Fe_3O_4 nanoparticles were embedded on SGO nanosheets and dispersed on the surface of the SGO nanosheets. As shown in Fig. 5c, no free Fe_3O_4 nanoparticles are detected outside of the SGO nanosheets, indicating the perfect combination between Fe_3O_4 and SGO nanosheets. The firmly attach of Fe_3O_4 nanoparticles to SGO nanosheets was confirmed by TEM images. The cross-sectional morphology images of M_S , M_{SP} , and M_{SPSF5} membranes are shown in Fig. 6. As shown in Fig. 6a, M_S membrane has smooth morphology, illustrating a strong cohesive force between the SPEEK chains, and when blended with PVA, surface roughness is found as showed in Fig. 6b confirming the presence of PVA. It is noteworthy that when SGO/ Fe_3O_4 nanosheets are dispersed in blend membrane, the sheet structure of SGO distributed through matrix of membrane due to formation of hydrogen bonding between SGO/ Fe_3O_4 nanosheets and blend membrane. The good dispersion of SGO/ Fe_3O_4 nanosheets in blend membrane is clearly observed in Fig. 6c.

Ion Exchange capacity, water uptake and membranes swelling

The ion-exchange capacity (IEC), water uptake and swelling properties are very important parameters for proton conducting polymer membranes. IEC is one of essential parameters for membrane which shows ability of ion exchanging and ion transferring of membrane. IEC is

an indicator of the density of proton exchangeable groups in the membrane. The IEC value for M_S and nanocomposite membranes was measured and results are shown in Table 1. As shown in Table 1, M_S membrane has maximum IEC before its blend with PVA polymer which is for absence of proton exchangeable groups ($-\text{SO}_3\text{H}$) in structure of PVA and consumed of $-\text{SO}_3\text{H}$ groups of SPEEK during cross-linking reaction. Gradual increase in IEC is observed as the content of SGO/ Fe_3O_4 nanosheets increases in the M_{SP} blend membrane, which is due to presence of $-\text{SO}_3\text{H}$ groups in structure of SGO/ Fe_3O_4 nanosheets. The higher amount of IEC increases proton conductivity in PEMs because of decrease in distance between proton exchangeable groups in membrane.

The membrane swelling is another important parameter to assess the dimensional stability of PEMs. The membranes with a high membrane swelling, lead to poor mechanical stability, high methanol permeability, low durability and decrease in fuel cell performance. The excessive membrane swelling results in membrane fragility which leads to weakness of nanocomposite membrane when incorporated into MEA.⁴² The M_S membrane exhibits lowest membrane swelling (14.9%) at room temperature (Table 1). In our previous work, the cross-linked PVA membrane shows a membrane swelling about 30%.³¹ As shown in Table 1, addition of PVA to SPEEK increases membrane swelling, which may be because of the hydrophilic nature and high membrane swelling of PVA polymer. The membrane swelling of blend membranes decreases with increase in the percentage of SGO/ Fe_3O_4 nanosheets in membrane. It shows that the hydrogen bonding between functionalized groups of nanosheets and blend membranes lead to more compact structure of membranes and increase rigidity of membranes and decrease membrane swelling. The M_{SPSF5} membrane exhibits higher membrane swelling (18.1%) than Nafion 117 (13.4%).²⁶

Water molecules are essential for proton transferring in membranes.²⁴ The available water molecules have an important role in proton conductivity of membrane with both proton transferring mechanism of Vehicle mechanism and Grotthuss mechanism. The water uptake of different prepared membranes is shown in Table 1. The water uptake of M_S membrane was 38% and was increased to 52.1% by blending with PVA. The reason of this phenomenon is more hydrophilic nature of PVA compared with SPEEK. The results of Table 1 show that the water uptake increased with increasing the SGO/Fe₃O₄ nanosheets content in blend membrane in order of M_{SPSF5} (58.3%) > M_{SPSF3} (54.6%), which may be the result of formation of hydrogen bonding between surface oxygen functionalized groups of nanosheets and free water.³¹ The hydrophilic nature of –SO₃H groups of SGO helped to increase water uptake. When the –SO₃H groups of SGO/Fe₃O₄ nanosheets were added to blend polymer, difference in the hydrophilic domains increased, creating broader channels with dead ends which causes water uptake improvement to occur.⁴⁰ As shown in Table 1, a further increase in SGO/Fe₃O₄ nanosheets content does not improve water uptake, which is due to aggregation of nanosheets in structure of blend membrane. This phenomenon is common in nanocomposites. The higher IEC and water uptake promote the proton conductivity due to essential role of them in proton transferring mechanisms. The water uptake of the M_{SPSF5} membrane (58.3%) is much higher than that of Nafion 117 (18.7%) in same condition.⁴³

Proton conductivity

Proton conductivity is the most important parameter for a PEM determining DMFC performance. In PEMs, two kinds of proton transport mechanism exist. At first, protons transfer by means of hopping from one proton conducting site (H₃O⁺ SO₃⁻) to another and named Grotthuss mechanism. At second, protons attach to free water molecules and diffuse as a whole through membrane and named Vehicle mechanism.

The Nyquist plots of prepared membranes at room temperature are shown in Fig. 7 and the proton conductivity results were summarised in Table 1. The proton conductivity of M_S membrane is 0.042 S cm^{-1} and reduced to 0.007 S cm^{-1} when blended with PVA, because of reduction on amount of $-\text{SO}_3\text{H}$ groups in membrane. The higher IEC of M_S membrane provides more acidic groups inside the membrane for proton transferring. As shown in Table 1, the proton conductivity of nanocomposite membranes increased with increasing SGO/ Fe_3O_4 content until 5 wt% in blend membrane. In the M_{SPSFX} nanocomposite membranes, the sulfonic acid groups of SGO can interact with free water molecules, forming a network of hydrogen bonds and increase proton conductivity of membrane by Grotthus mechanism. In addition, the surface hydroxyl groups of Fe_3O_4 nanoparticles can create hydrogen bonding with free water and increase proton conductivity via the Vehicle mechanism.¹³ The $-\text{SO}_3\text{H}$ groups of SPEEK are prone to attachment to SGO/ Fe_3O_4 surface, resulting in a very ordered structure with influence on the proton conducting pathway of membrane. With addition of 7 wt% SGO/ Fe_3O_4 nanosheets to blend membrane proton conductivity decreased, which was because of decrease of water uptake in this membrane and obstructed of polymer chain movement in proton cluster with addition of too many planar nanosheets.²²

Fig. 8 shows the Arrhenius plot of proton conductivity for different prepared membranes at temperature range of 25 to 100°C . The proton conductivity of all prepared membranes improves by increasing the temperature, because of increase in mobility of polymer chains and water molecules in higher temperature.⁴⁴ All of the prepared membranes showed highest proton conductivity at 80°C . At temperature above 80°C , the proton conductivity of membranes decreased due to evaporation of water in membrane. The bound water doesn't evaporate easily at high temperature. The high water uptake of prepared membranes can prevent from intensely decrease of proton conductivity in high temperature. The activation

energy (E_a) of the membranes was calculated according to the Arrhenius equation from temperature-dependent proton conductivity. The E_a of M_S , M_{SP} , M_{SPSF3} , M_{SPSF5} , and M_{SPSF7} membrane is 7.9, 9.6, 7.1, 6.4 and 6.9 kJ mol^{-1} , respectively. The decline of activation energy in M_{SPSF5} membrane suggested the decreased energy barrier for proton transfer in this membrane. The M_{SPSF5} membrane selected for more analyzed due to the highest water uptake and proton conductivity.

Methanol permeability and selectivity

The high methanol barrier property of membranes is essentially for DMFCs for reduction of catalyst poisoning and increase of membrane performance. Therefore, for practical uses of PEMs in DMFCs, it should have low methanol permeability. To make sure that the prepared membranes are suitable for DMFC application, the methanol permeability of M_S , M_{SP} , and M_{SPSF5} membranes were measured as a function of time at room temperature and results are shown in Table 2. The results of Table 2 show that the M_S membrane has the lowest methanol permeability ($7.36 \times 10^{-7} \text{ cm}^2 \text{ s}^{-1}$) compared to other membranes, because of its low membrane swelling. The higher membrane swelling increases ionic transport channels in membrane and increases methanol passing in membrane. Generally, The SPEEK shows low methanol permeability because of the less-pronounced hydrophilic-hydrophobic separation of highly branched structure of SPEEK.⁴⁵ The methanol permeability increased to $1.78 \times 10^{-6} \text{ cm}^2 \text{ s}^{-1}$ with addition of PVA to M_S membrane. This result may be arisen from that the hydrophilic natures of PVA render the membrane more hydrophilic, which could help methanol pass into the membrane. The higher water uptake of M_{SP} membrane allows more methanol to pass through along with water in this membrane.⁴⁶ As results of Table 2, the methanol permeability of M_{SP} blend membrane decreased from $1.78 \times 10^{-6} \text{ cm}^2 \text{ s}^{-1}$ to $8.83 \times 10^{-7} \text{ cm}^2 \text{ s}^{-1}$ with addition of 5 wt% SGO/ Fe_3O_4 nanosheets. The 101% decreases of methanol

permeability observed due to fuel barrier properties of graphene based nanosheets. Also, the transport channels were further narrowed in M_{SPSF5} membrane by the formation of hydrogen bond between hydroxyl, carboxylic and sulfonic groups of SGO/ Fe_3O_4 nanosheets and hydroxyl and sulfonic groups of blend polymer, thus methanol permeability of them is lower than M_{SP} membrane.

The proton conductivity and methanol permeability could greatly influence the performance of membranes in DMFCs. The selectivity of membranes is defined as the ratio of proton conductivity to methanol permeability and used to evaluate the potential performance of PEMs in DMFC applications. The PEMs applied in DMFCs should possess simultaneously low methanol permeability and high proton conductivity. As shown in Table 2, the selectivity of M_{SP} membrane is lower than other membranes due to lower proton conductivity and higher methanol permeability. The M_{SPSF5} membrane shows better selectivity than M_{S} membrane because of significant higher proton conductivity and little higher methanol permeability.

Mechanical properties and thermal stability

Besides its high proton conductivity, PEMs should serve several functions such as good thermal stability and appropriate mechanical properties for use in DMFCs. Fig. 9 shows the stress–strain behavior of the prepared membranes at room temperature and evaluated the tensile strength (TS) and elongation at break (E_b) of these membranes. The TS and E_b of the M_{S} membrane (TS: 18.72 MPa and E_b : 11.51%) is much lower than that of PVA membrane, which is 48.5 MPa and 174.75%, respectively.³¹ The M_{SP} membrane show increased TS and E_b (TS: 33.41 MPa and E_b : 66.88%) compared with M_{S} membrane, resulting from the better mechanical properties of PVA, increase in flexibility and enhanced intermolecular forces between polymers chains with cross–linking reaction. It can be clearly observed from Fig. 9 that the M_{SPSF5} membrane (TS: 51.76 MPa) shows better TS than M_{SP} membrane. It is

noteworthy that addition of SGO/Fe₃O₄ nanosheets to the blend membrane improves the TS of membrane due to remarkable mechanical properties of GO based nanosheets and formation of hydrogen bonding between functionalized groups of nanosheets and blend membranes.³¹ But, The E_b of blend membrane decreased with addition of SGO/Fe₃O₄ nanosheets (E_b: 34.08%), because of decrease in flexibility of polymer chains by incorporation with rigid SGO/Fe₃O₄ nanosheets. The results shows TS in M_{SPSF5} membrane (51.76 MPa) at room temperature is much higher than that of Nafion 117 (34.00 MPa) at same temperature.¹⁵

The thermal behavior of prepared membranes was investigated by DSC analysis. The DSC curves of M_S, M_{SP}, and M_{SPSF5} membrane are shown in Fig. 10. The M_S membrane shows a glass transition temperature (T_g) at about 173°C. The PVA is semi-crystalline polymer with T_g at 78°C and melting temperature (T_m) at 220°C.⁴⁷ As can be seen from Fig. 10, addition of PVA into the M_S membrane decreased the T_g of the blend membrane (T_g=166°C) corresponding to lower T_g of PVA and the promotes the chain motion of SPEEK.⁴⁸ Increase in flexibility of blend membranes confirmed by mechanical test. As shown in Fig. 10, the M_{SPSF5} membrane (T_g= 186°C) shows higher T_g compared to M_S and M_{SP} membrane. The T_g improvement was because of the increase of intermolecular interaction with formation of hydrogen bonding between nanosheets and blend membrane.⁴⁰ Also, increase in rigidity of M_{SPSF5} membrane with addition of rigid SGO/Fe₃O₄ nanosheets is another reason for increases of T_g in this membrane.

DMFC and Stability tests

Fig. 11 shows the potential-current polarization and power density curves of membranes in a DMFC operating at different temperature. Fig. 11a shows the cell polarization data for different membranes at 30°C. As shown in Fig. 11a, the DMFC based on M_S membrane has a

maximum peak power density of 36.12 mW cm^{-2} with maximum current density of 194.1 mA cm^{-2} while the DMFC equipped with the M_{SP} membrane has a maximum peak power density of 20.74 mW cm^{-2} with maximum current density of 134.7 mA cm^{-2} . The incorporation of the PVA into the SPEEK membrane decreases the performance of the DMFCs, which resulting from the increased methanol permeability and decreased proton conductivity of blend membrane. Peak power density of 47.17 mW cm^{-2} with maximum current density of 230.3 mA cm^{-2} is observed for M_{SPSF5} membrane which is higher in comparison with M_S and M_{SP} membrane. This can be assigned to the increased water uptake and proton conductivity of M_{SPSF5} membrane compared to M_S and M_{SP} membrane. Fig. 11b shows the cell polarization data of the M_{SPSF5} membrane at different temperature. The maximum peak power density of the M_{SPSF5} membrane is 47.17 , 87.11 , and 122.7 mW cm^{-2} with maximum current density of 230.3 , 305.3 , and 381.9 mA cm^{-2} at 30 , 60 , and 80°C , respectively. These results showed the improved performance of the M_{SPSF5} membrane with increase of temperature which was because of increases of proton conductivity with increase of temperature (Fig. 8). However, M_{SPSF5} membrane shows superior power density as well as current density compared to other membranes which is in agreement with other results stated above.

The long term stability test is an evaluation of voltage decay and membrane degradation in DMFC versus time. The long term stability of the different membranes in DMFC was investigated at open circuit voltage (OCV) and results are shown in Fig.12. The results show the OCV reduction rate for about 120 h in M_S , M_{SP} and M_{SPSF5} membranes are 0.85 mV h^{-1} , 0.71 mV h^{-1} and 0.65 mV h^{-1} , respectively. The better mechanical stability of M_{SPSF5} membrane helps lower voltage decay in this membrane compared to M_S and M_{SP} membranes. However, all of synthesized membranes showed good stability in DMFC operation during long time.

Conclusions

The nanocomposite blend membranes based on SPEEK/PVA blend polymers and SGO/Fe₃O₄ nanosheets were prepared by solution casting method. The structure of prepared nanosheets and membranes were confirmed by XRD, FTIR, SEM, and TEM study. Compared with M_S membrane, the blend M_{SP} membrane shows an enhanced water uptake and mechanical properties. Addition of SGO/Fe₃O₄ nanosheets to blend membrane improved mechanical stability, methanol barrier properties, proton conductivity and power density of membranes. The sulfonic acid groups of SGO nanosheets may provide the additional bridge with polymers matrix for proton transport through nanocomposite membrane. A literature survey on proton conductivity, methanol permeability, and power density of Nafion 117 and SPEEK-based membranes is presented in Table 3. The proton conductivity and methanol permeability of the M_{SPSF5} membranes is comparable to that of other membranes. It is interesting to note from Table 3 that M_{SPSF5} membrane showed higher power density than Nafion 117 and other SPEEK-based blend and composite membranes reported in the literature at same temperature. These results showed that the M_{SPSF5} membrane is a good methanol separator and great proton carrier and thus, this membrane is promising to be used as PEM in DMFCs.

Acknowledgement

The authors are grateful to the Renewable Energy Research Center (Amirkabir University of Technology, Tehran, Iran) for the financial support of this work.

References

1. C. C. Yang, Y. J. Lee and J. M. Yang, *J. Power Sources*, 2009, **188**, 30.
2. S. Gahlot, P. P. Sharma, H. Gupta, V. Kulshrestha and P. K. Jha, *RSC Adv.*, 2014, **4**, 24662.
3. Y.-H. Cho, J. W. Bae, O. H. Kim, J. Y. Jho, N. Jung, K. Shin, H. Choi, H. Choe, Y. H. Cho and Y. E. Sung, *J. Membr. Sci.*, 2014, **467**, 36.
4. H. Beydaghi, M. Javanbakht and A. Badiei, *J. Nanostru. Chem.*, 2014, **4**, 1.
5. S. P. Cabello, S. Molla, N. Ochoa, J. Marchese, E. Gimenez and V. Compan, *J. Power Sources*, 2014, **265**, 345.
6. S. K. Kamarudin, F. Achmad and W. R. W. Daud, *Int. J. Hydrogen Energy*, 2009, **34**, 6902.
7. Y. Oh, S. K. Kim, D. H. Peck, D. H. Jung and Y. Shul, *Int. J. Hydrogen Energy*, 2014, **39**, 15760.
8. T. Yuan, L. Pu, Q. Huang, H. Zhang, X. Li and H. Yang, *Electrochim. Acta*, 2014, **117**, 393.
9. P. Salarizadeh, M. Javanbakht, M. Abdollahi and L. Naji, *Int. J. Hydrogen Energy*, 2013, **38**, 5473.
10. K. Hooshyari, M. Javanbakht, A. Shabanikia and M. Enhessari, *J. Power Sources*, 2015, **276**, 62.
11. P. Salarizadeh, M. Abdollahi and M. Javanbakht, *Iranian Polym. J.*, 2012, **21**, 661.
12. A. Shabanikia, M. Javanbakht, H. S. Amoli, K. Hooshyari and M. Enhessari, *J. Electrochem. Soc.*, 2014, **161**, 1403.
13. K. Hooshyari, M. Javanbakht, L. Naji and M. Enhessari, *J. Membr. Sci.*, 2014, **454**, 74.
14. R. Silva, S. Passerini and A. Pozio, *Electrochim. Acta*, 2005, **50**, 2639.

15. J. Pandey, F. Q. Mir and A. Shukla, *Int. J. Hydrogen Energy*, 2014, **39**, 9473.
16. F. Ding, S. Wang, M. Xiao and Y. Meng, *J. Power Sources*, 2007, **164**, 488.
17. Y. M. Sun, T. C. Wu, H. C. Lee, G. B. Jung, M. D. Guiver, Y. Gao, Y. L. Liu and J. Y. Lai, *J. Membr. Sci.*, 2005, **265**, 108.
18. A. Shabanikia, M. Javanbakht, H. S. Amoli, K. Hooshyari and M. Enhessari, *Electrochim. Acta*, 2015, **154**, 370.
19. T. H. Tang, P. H. Su, Y. C. Liu and T. L. Yu, *Int. J. Hydrogen Energy*, 2014, **39**, 11145.
20. Y. M. Ferng, A. Su and J. Hou, *Energy Convers. Manage.*, 2014, **78**, 431.
21. S. C. Gil, J. C. Kim, D. Ahn, J. S. Jang, H. Kim, J. C. Jung, S. Lim, D. H. Jung and W. Lee, *J. Membr. Sci.*, 2012, **417**, 2.
22. Klaysom, B. P. Ladewig, G. M. Lu and L. Wang, *J. Membr. Sci.*, 2011, **368**, 48.
23. A. M. Attaran, M. Javanbakht, K. Hooshyari and M. Enhessari, *Solid State Ionics*, 2015, **269**, 98.
24. H. Beydaghi, M. Javanbakht, H. S. Amoli, A. Badieli, Y. Khaniani, M. R. Ganjali, P. Norouzi and M. Abdouss, *Int. J. Hydrogen Energy*, 2011, **36**, 13310.
25. R. Narducci, M. D. Vona and P. Knauth, *J. Membr. Sci.*, 2014, **465**, 185.
26. Y. Liang, C. Gong, Z. Qi, H. Li, Z. Wu, Y. Zhang, S. Zhang and Y. Li, *J. Power Sources*, 2015, **284**, 86.
27. Y. Heo, H. Im and J. Kim, *J. Membr. Sci.*, 2013, **425**, 11.
28. G. Rambabu and S. D. Bhat, *Chem. Eng. J.*, 2014, **243**, 517.
29. Z. Jiang, X. Zhao and A. Manthiram, *Int. J. Hydrogen Energy*, 2013, **38**, 5875.
30. S. Molla and V. Compan, *Int. J. Hydrogen Energy*, 2014, **39**, 5121.
31. H. Beydaghi, M. Javanbakht and E. Kowsari, *Ind. Eng. Chem. Res.*, 2014, **53**, 16621.

32. P. P. Sharma, S. Gahlot, B. M. Bhil, H. Gupta and V. Kulshrestha, *RSC Adv.*, 2015, **5**, 38712.
33. X. H. Beydaghi and M. Javanbakht, *Ind. Eng. Chem. Res.*, 2015, **54**, 7028.
34. W. S. Hummers Jr and R. E. Offeman, *J. Am. Chem. Soc.*, 1958, **80**, 1339.
35. R. N. Muthu, S. Rajashabala and R. Kannan, *Int. J. Hydrogen Energy*, 2015, **40**, 1836.
36. B. Tosh, C. Saikia and N. Dass, *J. appl. Polym. Sci.*, 1999, **74**, 663.
37. S. Gahlot, P. P. Sharma, V. Kulshrestha and P. K. Jha, *ACS Appl. Mater. Interfaces*, 2014, **6**, 5595.
38. A. M. Baker, L. Wang, S. G. Advani and A. K. Prasad, *J. Mater. Chem.*, 2012, **22**, 14008.
39. M. Yadav, K. Y. Rhee, S. J. Park and D. Hui, *Composites Part B: Engineering*, 2014, **66**, 89.
40. A. Mayahi, A. Ismail, H. Ilbeygi, M. Othman, M. Ghasemi, M. M. Norddin and T. Matsuura, *Sep. Purif. Technol.*, 2013, **106**, 72.
41. T. Yang, *Int. J. Hydrogen Energy*, 2008, **33**, 6772.
42. R. Padmavathi and D. Sangeetha, *Ionics*, 2013, **19**, 1423.
43. H. Ch. Chien, L. D. Tsai, Ch. P. Huang, Ch. Y. Kang, J. N. Lin and F. Ch. Chang, *Int. J. Hydrogen Energy*, 2013, **38**, 13792.
44. N. Cele and S. S. Ray, *Macromol. Mater. Eng.*, 2009, **294**, 719.
45. S. Sasikala, S. Meenakshi, S. Bhat and A. Sahu, *Electrochim. Acta*, 2014, **135**, 232.
46. H. Wu, Y. Cao, Z. Li, G. He and Z. Jiang, *J. Power Sources*, 2015, **273**, 544.
47. C. P. Liu, C. A. Dai, C. Y. Chao and S. J. Chang, *J. Power Sources*, 2014, **249**, 285.
48. J. Wang, Z. Zhang, X. Yue, L. Nie, G. He, H. Wu and Z. Jiang, *J. Mater. Chem. A*, 2013, **1**, 2267.

49. H. Ilbeygi, A. F. Ismail, A. Mayahi, M. M. Nasef, J. Jaafar and E. Jalalvandi, *Sep. Purif. Technol.*, 2013, **118**, 567.
50. J. Ch. Tsai, Ch. K. Lin, *J. the Taiwan Inst. Chem. E.*, 2011, **42**, 281.
51. Zh. Jiang, X. Zhao, Y. Fu and A. Manthiram, *J. Mater. Chem.*, 2012, **22**, 24862.
52. J. Ch. Tsai, Ch. K. Lin, *J. Power Sources*, 2011, **196**, 9308.
53. Q. He, J. Zheng and S. Zhang, *J. Power Sources*, 2014, **260**, 317.

Figure legends

Fig. 1. Structure and ^1H NMR spectrum of SPEEK

Fig. 2. (a) Three-dimensional presumptive representation structure of cross-linked M_{SPSF_x} membrane, (b) Three-dimensional and (c) Two-dimensional schematic illustration for interaction between polymeric chains and nanosheets

Fig. 3. XRD patterns of the GO, SGO, and SGO/ Fe_3O_4 nanosheets and Fe_3O_4 nanoparticles

Fig. 4. FTIR spectra of SGO/ Fe_3O_4 nanosheets and M_{S} , M_{SP} and M_{SPSF_5} membranes

Fig. 5. SEM and TEM images of the (a,b) SGO and (c,d) SGO/ Fe_3O_4 nanosheets

Fig. 6. The cross-sectional SEM images of (a) M_{S} (b) M_{SP} and (c) M_{SPSF_5} membranes

Fig. 7. Nyquist plots of prepared membranes at fully hydrated condition

Fig. 8. Arrhenius plot of the proton conductivity for prepared membranes

Fig. 9. Stress-strain curves of the M_{S} , M_{SP} and M_{SPSF_5} membranes

Fig. 10. DSC curves of M_{S} , M_{SP} and M_{SPSF_5} membranes

Fig. 11. Current density–potential (I–V) and power density curves of the DMFC assembled with (a) different prepared membranes at 30°C and (b) M_{SPSF_5} membrane at different temperatures.

Fig. 12. OCV behavior of the DMFC assembled with the membranes at 30°C

Table 1. Comparison of the ion-exchange capacity (IEC), water uptake (WU), membrane swelling (SW), and proton conductivity (σ) of the prepared membranes at 30 °C

Membrane	IEC (meq g ⁻¹)	WU (%)	SW (%)	σ (S cm ⁻¹)
M _S	1.6	38	14.9	0.042
M _{SP}	0.91	52.1	21.1	0.007
M _{SPSF3}	1.11	54.6	19.8	0.068
M _{SPSF5}	1.32	58.3	18.1	0.084
M _{SPSF7}	1.43	56.9	17.7	0.076

Table 2. Comparison of the proton conductivity (σ), methanol permeability (P), and selectivity (S) of the prepared membranes

Membranes	σ (S cm ⁻¹)	P (cm ² s ⁻¹)	S (S s ⁻¹ cm ⁻³)
M _S	0.042	7.36×10^{-7}	5.70×10^4
M _{SP}	0.007	1.78×10^{-6}	3.932×10^3
M _{SPSF5}	0.084	8.83×10^{-7}	9.51×10^4

Table 3. Comparison of the proton conductivity (σ), methanol permeability (P), and power density (PD) of the M_{SPSF5} membrane with Nafion 117 and SPEEK based membranes used in DMFC

Membranes	Temperature ($^{\circ}\text{C}$)	σ (S/cm)	P ($\text{cm}^2 \text{s}^{-1}$)	PD (mW cm^{-2})	Ref
M_{SPSF5}	30	0.084	8.83×10^{-7}	47.17	This work
M_{SPSF5}	60	0.122	-	87.11	This work
M_{SPSF5}	80	0.139	-	122.7	This work
SPEEK/SSi-GO ^a	65	0.160	0.83×10^{-6}	72.2	[29]
SPEEK/CC/TAP ^b	60	0.047	0.29×10^{-6}	54.93	[49]
SPEEK/PSSA/CNTs ^c	60	0.101	2.17×10^{-7f}	93	[28]
aminated SPEEK/Nafion	30	0.063	8.92×10^{-7}	26	[50]
SPEEK/SDBS-GO ^d	65	0.155	0.82×10^{-6f}	63	[51]
MS-SPEEK ^e	80	0.12	3.26×10^{-6}	115	[52]
Nafion 117	30	0.09	2.4×10^{-6}	24	[53]

^a Sulfonated organosilane functionalized graphene oxide; ^b Cloisite 15A clay compatibilized with 2,4,6-triaminopyrimidine; ^c Polystyrene sulfonic acid functionalized multi-walled carbon nanotubes; ^d Sodium dodecylbenzene sulfonate adsorbed graphene oxide; ^e SPEEK with 2-aminoethanesulphonic acid; ^f measured at room temperature.

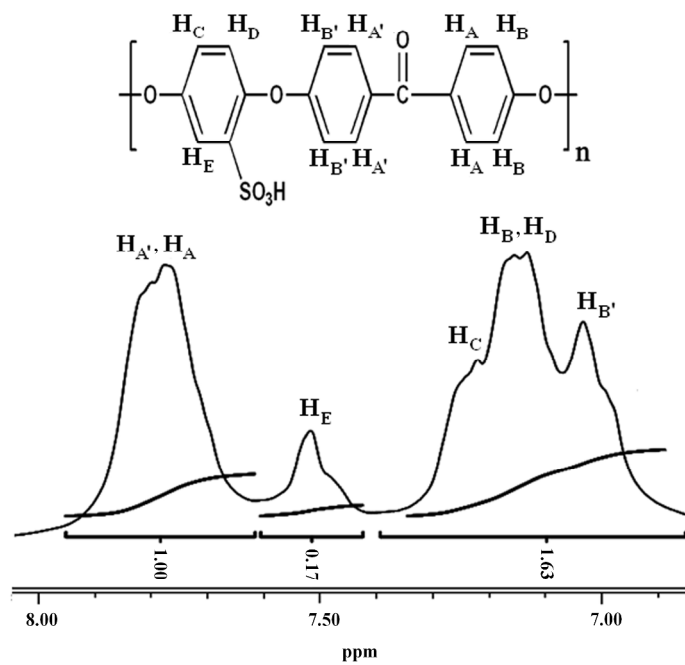
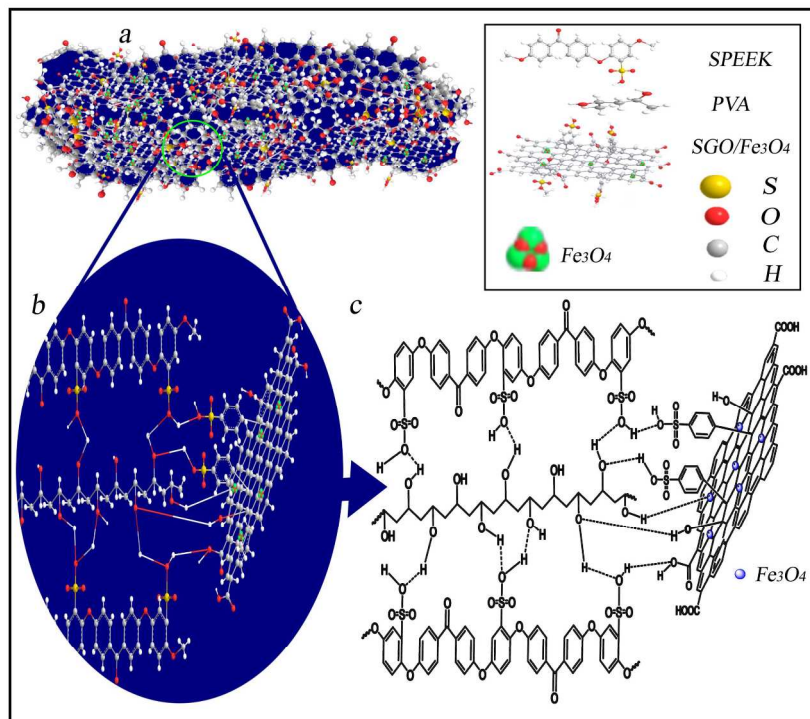


Fig. 1

282x352mm (300 x 300 DPI)

**Fig. 2**

296x419mm (300 x 300 DPI)

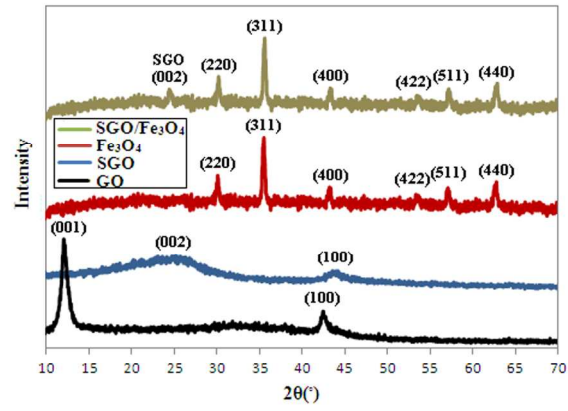


Fig. 3

211x264mm (300 x 300 DPI)

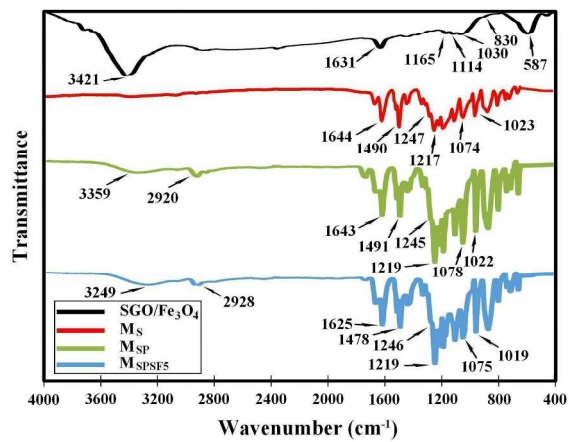


Fig. 4

209x297mm (300 x 300 DPI)

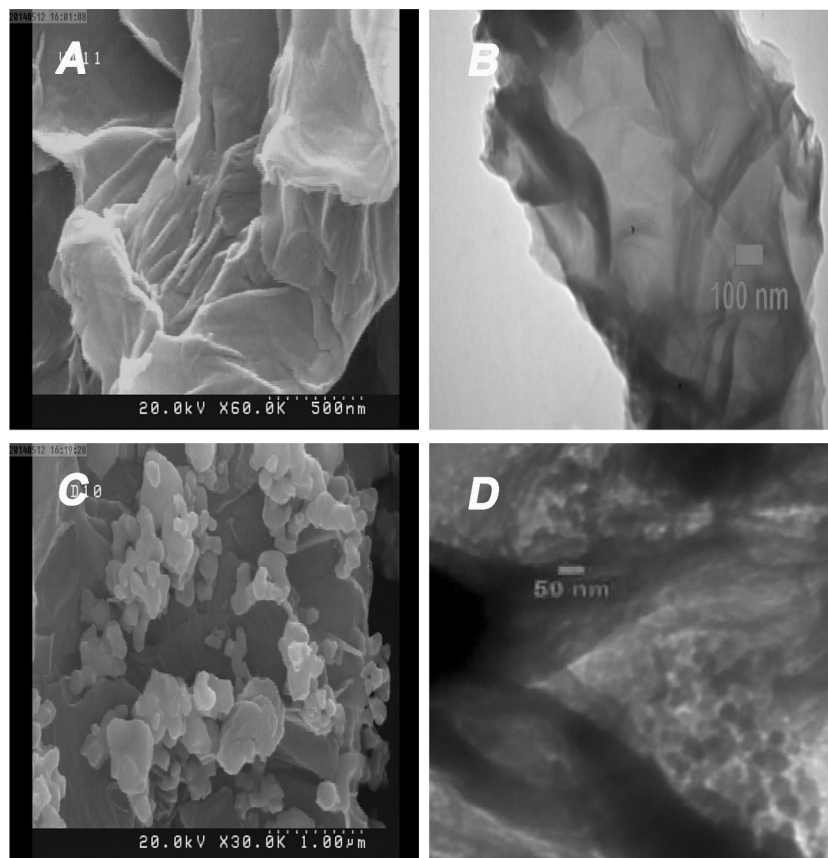


Fig. 5

656x928mm (96 x 96 DPI)

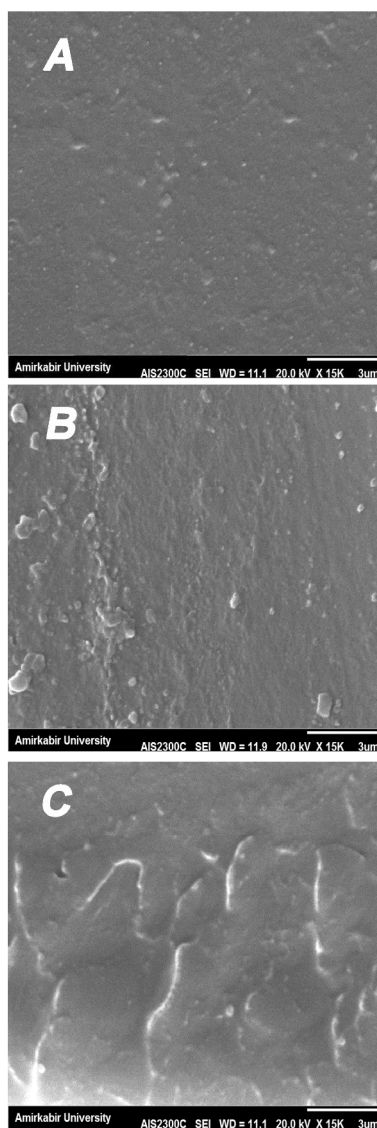


Fig. 6

874x1237mm (72 x 72 DPI)

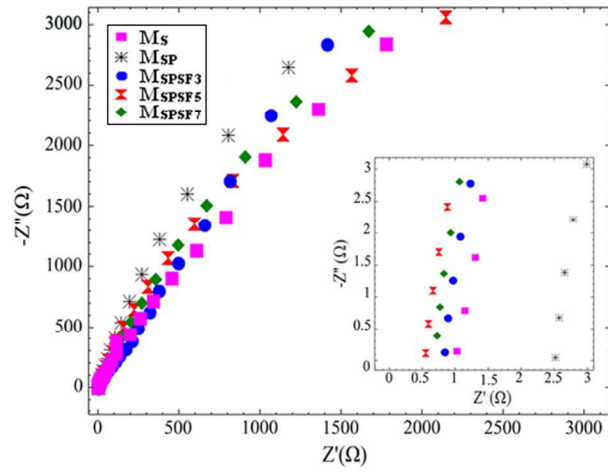
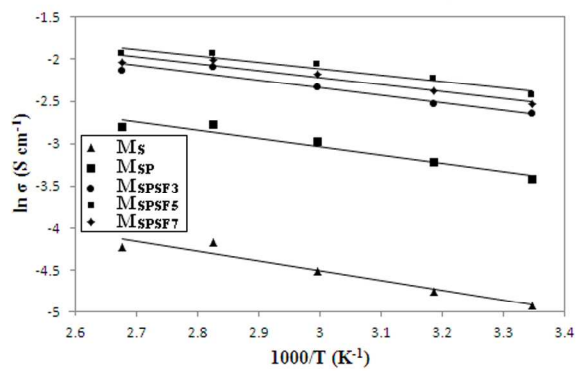


Fig. 7

282x352mm (300 x 300 DPI)

**Fig. 8**

282x352mm (300 x 300 DPI)

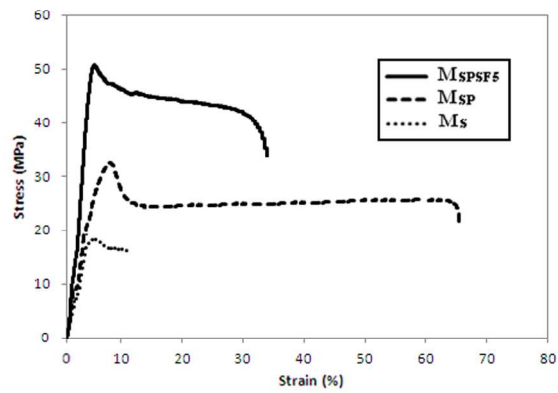


Fig. 9

282x352mm (300 x 300 DPI)

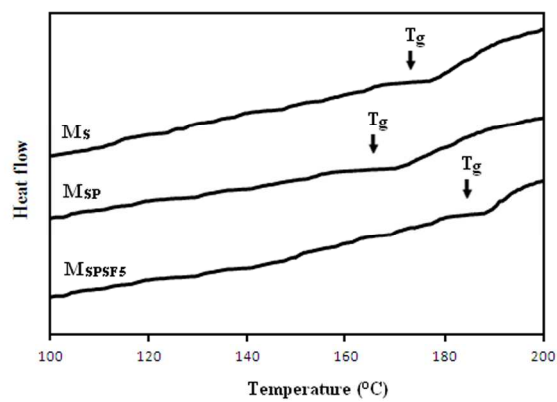


Fig.10

211x264mm (300 x 300 DPI)

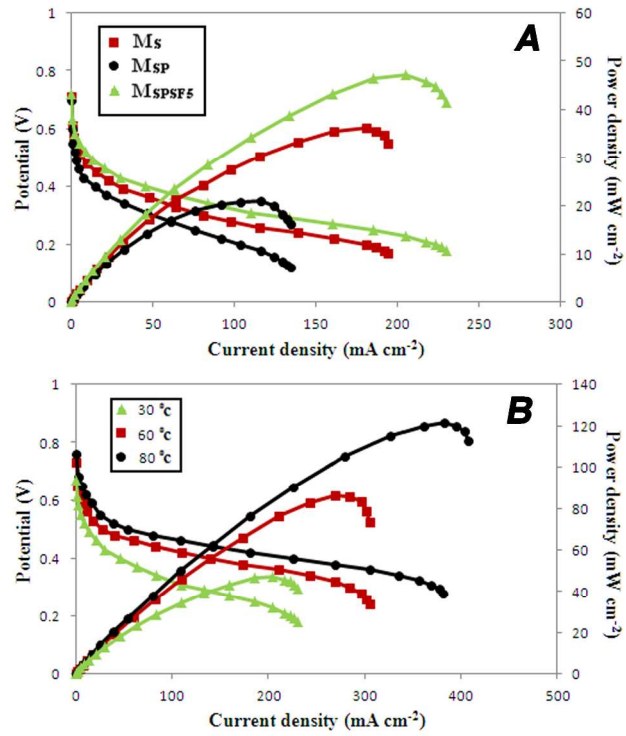


Fig.11

282x352mm (300 x 300 DPI)

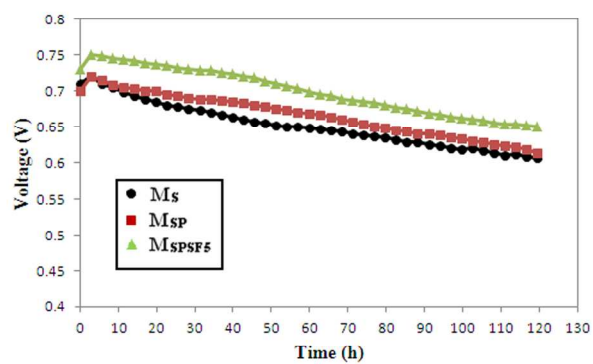


Fig. 12

282x352mm (300 x 300 DPI)